

Measurement of the W^+W^- Cross Section in $\sqrt{s} = 7$ TeV pp Collisions with the ATLAS Detector

Haijun Yang (on behalf of the ATLAS Collaboration)
 Department of Physics, University of Michigan, Ann Arbor, MI 48109-1120, USA

We report a measurement of the W^+W^- production cross section in pp collisions at $\sqrt{s} = 7$ TeV. The W^+W^- leptonic decay channels are analyzed using data corresponding to 1.02 fb^{-1} of integrated luminosity collected by the ATLAS detector during 2011 at the CERN Large Hadron Collider. With 414 observed W^+W^- candidate events and an estimated background of 170 ± 28 events, the measured W^+W^- production cross section is $48.2 \pm 4.0(\text{stat}) \pm 6.4(\text{syst}) \pm 1.8(\text{lumi}) \text{ pb}$, in agreement with the Standard Model NLO prediction of $46 \pm 3 \text{ pb}$.

1. Introduction

The measurement of the W^+W^- production cross section at the LHC provides an important test of the Standard Model (SM) through the sensitivity to the triple gauge boson couplings that result from the non-Abelian structure of the gauge symmetry group, $SU(2)_L \times U(1)_Y$. Furthermore, non-resonant W^+W^- production is an irreducible background in searches for the Higgs boson in the same final state. Understanding the detection sensitivity of ATLAS to W -pair production is crucial for Higgs boson searches. The WW cross section has been measured at LHC with the ATLAS detector using limited statistics based on 2010 data (34 pb^{-1}) [1], this paper presents new results with 1.02 fb^{-1} integrated luminosity collected in 2011.

Candidate W^+W^- events are reconstructed in the leptonic decay channels, $W^\pm \rightarrow \ell^\pm \nu$, where ℓ is an electron or muon. Sequential decays to electrons and muons via τ leptons are also included as signal: $W^\pm \rightarrow \tau^\pm \nu_\tau \rightarrow \ell^\pm \nu_\ell \nu_\tau \bar{\nu}_\tau$. The resulting final state has two high-transverse-momentum (high- p_T) charged leptons and substantial transverse momentum imbalance in the final state (referred to as missing transverse energy E_T^{miss} below) due to the neutrinos or antineutrinos escaping detection. The major backgrounds for this $\ell^+ \ell^- E_T^{\text{miss}}$ final state are Drell-Yan, top quark, W +jet and diboson (WZ , ZZ and $W\gamma$) production.

2. The ATLAS detector and data sample

The ATLAS detector [2] is a multipurpose particle physics apparatus with nearly 4π solid angle coverage. ATLAS uses a right-handed coordinate system with its origin at the nominal interaction point (IP) in the centre of the detector and the z -axis along the beam pipe. The x -axis points from the IP to the centre of the LHC ring, and the y axis points upward. Cylindrical coordinates (r, ϕ) are used in the transverse plane, ϕ being the azimuthal angle around the beam pipe. The pseudorapidity is defined in terms of the polar angle θ as $\eta = -\ln[\tan(\theta/2)]$. Closest to the beamline are inner tracking detectors which use layers of silicon-based and straw-tube detectors, located inside a thin superconducting solenoid that provides a 2T magnetic field, to measure the trajectories of charged particles within $|\eta| < 2.5$. The solenoid is surrounded by a hermetic calorimeter system. A liquid argon (LAr) sampling calorimeter is divided into a central barrel calorimeter and two end-cap calorimeters, each housed in a separate cryostat. Fine-grained LAr electromagnetic (EM) calorimeters, with excellent energy resolution, provide coverage for $|\eta| < 3.2$. An iron-scintillator tile calorimeter provides hadronic coverage in the range $|\eta| < 1.7$. In the end-caps ($|\eta| > 1.5$), LAr hadronic calorimeters match the outer $|\eta|$ limits of the end-cap EM calorimeters. LAr forward calorimeters provide both EM and hadronic energy measurements, and extend the coverage to $|\eta| < 4.9$. Outside the calorimeters is an extensive muon spectrometer in a toroidal magnetic field, providing precise muon measurements within $|\eta| < 2.7$. The muon trigger system covers the range $|\eta| < 2.4$.

A three-level trigger system is used to select interesting events in real time. The electron trigger selects electrons that deposit at least 20 GeV of transverse energy in the calorimeter. The muon trigger requirement consists of a logical OR between a trigger that requires a muon detected with a transverse momentum of at least 18 GeV and a looser quality trigger that requires a muon of at least 40 GeV in the barrel section of the muon spectrometer. The data used for this analysis were recorded up to June 2011 and correspond to an integrated luminosity of 1.02 fb^{-1} . The luminosity is determined with a relative uncertainty of 3.7% using van der Meer scans [3].

Monte Carlo simulation samples are used to develop and validate the analysis procedures, to calculate the acceptance for W^+W^- events and to evaluate the contributions from some background processes.

For the W^+W^- signal, we use the next-to-leading order (NLO) generator MC@NLO [4] in conjunction with the CTEQ6.6 [5] parton distribution functions (PDF). HERWIG [6] is used for W leptonic decays and for the parton shower simulation and hadronization. Jimmy [7] is used for the underlying event simulation. In addition, the gg2ww [8] MC generator (interfaced to HERWIG and Jimmy) is used to simulate the W^+W^- events from the gluon-gluon fusion process.

The Drell-Yan and the W + jets backgrounds are generated with ALPGEN. The top ($t\bar{t}$ and Wt) and diboson (WZ and ZZ) backgrounds are modeled with MC@NLO interfaced to the HERWIG and Jimmy programs. The single top background samples are produced with the AcerMC generator [10]. $W\gamma$ is modeled using PYTHIA/MADGRAPH [11], and hadronic multi-jet backgrounds with the PYTHIA generator.

The detector response for all the generated MC events is simulated by passing them through a detailed simulation [12] of the ATLAS detector based on the GEANT4 program [13]. These simulated data samples are then reconstructed, selected, and analyzed as it is done for the data.

3. Object reconstruction

Brief descriptions of the relevant physics objects used in this analysis are given in this section. These objects are the pp collision vertices, electrons, muons, missing transverse energy, and hadronic jets.

The pp collision vertices in each bunch crossing are reconstructed using the inner tracking system. To remove cosmic-ray and beam-induced backgrounds, we require the primary vertex to have three or more tracks.

Electron candidates are formed by matching a cluster of energy in the electromagnetic calorimeter to a charged track found in the inner tracking system. In this analysis, we use electrons with $|\eta| < 1.37$ or $1.52 < |\eta| < 2.47$, which avoids the transition region between the barrel and the end-cap electromagnetic calorimeters.

We use the ATLAS “tight” electron identification criteria [14]. The E_T of the leading electron in the ee channel and the E_T of the electron in the $e\mu$ channel are required to exceed 25 GeV. The sub-leading E_T in the ee channel must be greater than 20 GeV. The isolation requirement is that the sum of the energy in the calorimeter cells within a cone $\Delta R = \sqrt{(\Delta\eta)^2 + (\Delta\phi)^2}$ of 0.3 around the electron, excluding the energy in the electron cluster and after corrections for leakage and pileup effects, must be less than 4 GeV. In addition, the longitudinal impact parameter $|z_0|$ of the track relative to the primary vertex must be smaller than 10 mm, and the transverse impact parameter significance d_0/σ_{d_0} must be less than 10, where d_0 and σ_{d_0} are the transverse impact parameter relative to the primary vertex and its uncertainty, respectively. The electron identification efficiency is measured in data using control samples of $Z \rightarrow e^+e^-$ and $W^\pm \rightarrow e^\pm\nu$ events. The overall electron selection efficiency in this analysis is about 78% for the central region ($|\eta| < 0.8$), and decreases to about 64% in the endcap region ($2.0 < |\eta| < 2.47$).

Muons are reconstructed using information from the muon spectrometer, the inner tracking detectors, and the calorimeters. The absolute value of the pseudorapidity $|\eta|$ of the combined muon is required to be less than 2.4. The muon transverse momentum measured by combining information from the muon spectrometer and inner detector systems must be greater than 20 GeV. To suppress muons originating from hadronic jets, the muons must be isolated such that the p_T sum of other tracks in a cone of $\Delta R = 0.2$ around the muon track divided by the muon p_T is less than 0.1. The muon reconstruction and identification efficiencies are measured using $Z \rightarrow \mu^+\mu^-$ candidates in data. The overall muon reconstruction efficiency is found to be $92.8\% \pm 1.0\%$ (syst) in data with negligible statistical uncertainty.

Jets are reconstructed from calorimeter clusters using the anti- k_t algorithm [15–17] with a jet resolution parameter of $\Delta R = 0.4$. These jets are calibrated using p_T - and η -dependent correction factors [18] based on MC simulation, and validated by extensive test beam and collision data. The selected jets are required to have $p_T > 30$ GeV and $|\eta| < 4.5$. The jet energy scale uncertainty depends on p_T and η and ranges from 2% - 8% for $p_T > 30$ GeV and $|\eta| < 4.5$ due to calibration [18].

The missing transverse energy is reconstructed using calorimeter energies from clusters in the detection range $|\eta| < 4.5$ and muon momenta measured by the muon spectrometer and inner detector. The mis-measured energies of leptons or jets can produce false E_T^{miss} . To reduce the rate of backgrounds that arise from these mis-measurements, particularly the Drell-Yan background, we use a relative missing transverse energy ($E_{T, \text{Rel}}^{\text{miss}}$), which is defined as the following:

$$E_{T, \text{Rel}}^{\text{miss}} = \begin{cases} E_T^{\text{miss}} \times \sin(\Delta\phi_{\ell,j}) & \text{if } \Delta\phi < \pi/2 \\ E_T^{\text{miss}} & \text{if } \Delta\phi \geq \pi/2, \end{cases} \quad (1)$$

where $\Delta\phi_{\ell,j}$ is the difference in the azimuthal angle ϕ between the E_T^{miss} and the nearest lepton or jet. The asymmetric requirement on $E_{T, \text{Rel}}^{\text{miss}}$ helps to optimize the WW detection significance. This requirement also

reduces the background from $Z \rightarrow \tau^+\tau^-$, where the real $E_{T, \text{Rel}}^{\text{miss}}$ from the τ semileptonic decays is parallel to the momenta of the leptons.

4. Event selection

Di-lepton events are selected using the lepton identification requirements described in the previous section. For each di-lepton final state (ee , or $\mu\mu$, or $e\mu$), we require each electron (or muon) to have E_T (or p_T) > 20 GeV, and we require exactly two leptons with opposite charges. The electron in the $e\mu$ channel and the leading electron in the ee channel must have $E_T > 25$ GeV. Both leptons are required to originate from the primary vertex. At least one of the selected leptons is required to have fired its corresponding trigger (“trigger matching”). The leptons must also have a minimum separation (effectively imposed by the lepton isolation requirement) in $\eta - \phi$ space of $\Delta R > 0.3$ in the ee channel and $\Delta R > 0.2$ in the $\mu\mu$ and the $e\mu$ channels.

To reduce the Drell-Yan background and the background from hadronic multi-jets, the invariant mass of the dilepton pair (e^+e^- or $\mu^+\mu^-$) is required to exceed 15 GeV and is not allowed to be within ± 15 GeV of the Z -mass. In addition, the invariant mass of the dilepton pair ($e^-\mu^+$ or $e^+\mu^-$) is required to exceed 10 GeV.

As shown in Fig. 1, further suppression of the remaining Drell-Yan and other backgrounds is achieved by requiring $E_{T, \text{Rel}}^{\text{miss}} > 40$ GeV for the ee channel, $E_{T, \text{Rel}}^{\text{miss}} > 45$ GeV for the $\mu\mu$ channel and $E_{T, \text{Rel}}^{\text{miss}} > 25$ GeV for the $e\mu$ channel. To optimize the signal to background ratio, different $E_{T, \text{Rel}}^{\text{miss}}$ cuts are chosen for the different channels. The figure shows the $E_{T, \text{Rel}}^{\text{miss}}$ distribution prior to applying the jet-veto criteria for the ee , $\mu\mu$ and $e\mu$ channels.

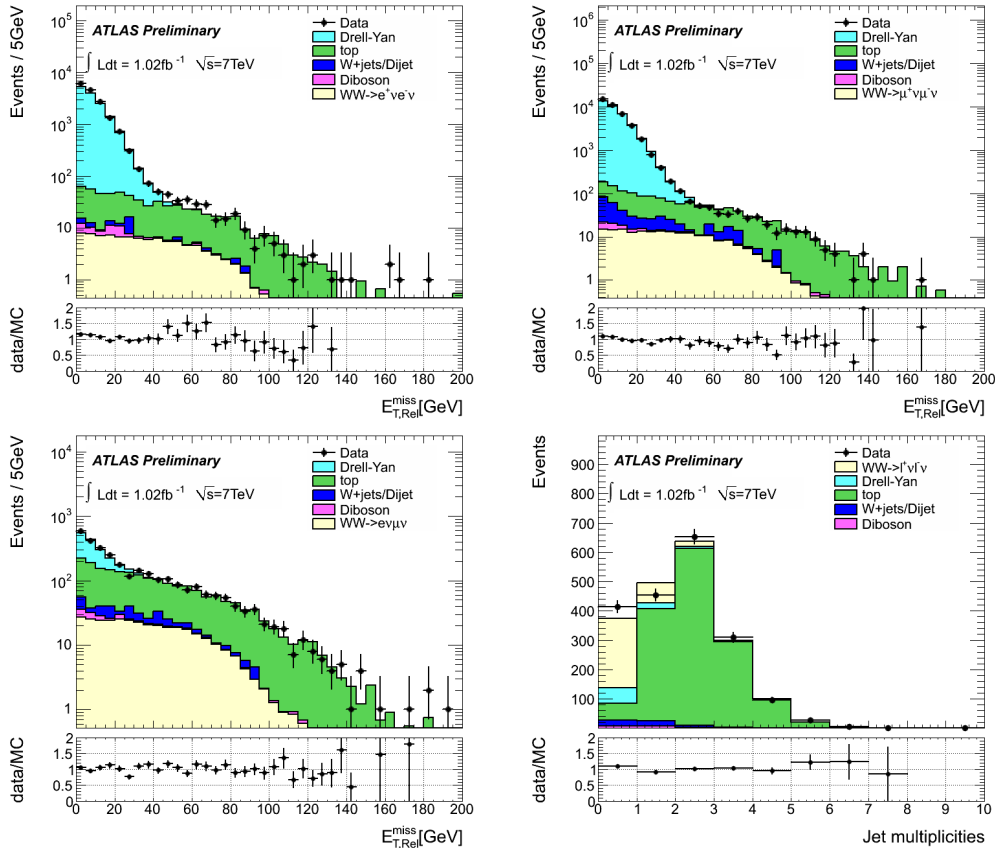


Figure 1: $E_{T, \text{Rel}}^{\text{miss}}$ distributions for the selected ee , $\mu\mu$ and $e\mu$ samples after the Z mass veto cut. Bottom right plot shows the jet multiplicity after $E_{T, \text{Rel}}^{\text{miss}}$ cut.

Suppression of the top background is accomplished by rejecting events containing jets with $p_T > 30$ GeV and $|\eta| < 4.5$ (the jet-veto requirement). Figure 1 shows that the majority of the W^+W^- signal is in the zero-jet bin of the jet multiplicity distribution, while the top events populate the higher jet multiplicity bins.

After all the selection criteria are applied to the di-lepton samples, 414 W^+W^- candidate events remain: 74 in the ee channel, 97 in the $\mu\mu$ channel, and 243 in the $e\mu$ channel.

The signal acceptance is one of the key ingredients for determining the W^+W^- cross section. Determining this acceptance relies on detailed MC signal modeling and event selection efficiency corrections using control data samples. These corrections differ by at most a few percent from unity, indicating the inherent accuracy of the simulation. Detailed information on the W^+W^- event selection acceptance is provided below. Table I shows the number of MC W^+W^- events passing each selection cut for the three di-lepton channels. The MC events shown in the table are normalized to 1.02 fb^{-1} using the SM W^+W^- production cross sections with $q\bar{q}'$ and gg initial states. In order to minimize the systematic uncertainty due to initial state radiation (ISR) and jet-energy scale, we use control samples of $Z \rightarrow \ell^+\ell^-$ data and MC to determine the jet-veto efficiency correction factor to the W^+W^- selection [19]: $\epsilon_{WW}^{\text{data}} = \epsilon_{WW}^{\text{MC}} \times f_Z$, with $f_Z = \epsilon_Z^{\text{data}}/\epsilon_Z^{\text{MC}} = 0.99 \pm 0.05$ (syst). The two efficiency numbers, ϵ_Z^{data} and ϵ_Z^{MC} , are the fraction of the Z events with zero jets found in data and MC, respectively. The main contributions to the given systematic uncertainty are due to factorisation and renormalisation scale choice evaluated using MC@NLO and MCFM [20]. The overall event selection acceptances for signal events are 5.0% for $e\nu e\nu$, 8.9% for $\mu\nu\mu\nu$, and 12.6% for $e\nu\mu\nu$ events. The contributions from $W^+W^- \rightarrow \tau^\pm\nu\ell^\mp\nu \rightarrow \ell'^\pm\ell'^\mp + n\nu$ are less than 8% of the final selected W^+W^- signal events in all three di-lepton channels. The overall systematic uncertainty in the W^+W^- selection acceptance is 6.8% for the combination of the three di-lepton channels. This overall uncertainty includes the uncertainties due to lepton identification (4.2%), the jet-veto (4.8%), the $E_{\text{T, Rel}}^{\text{miss}}$ uncertainty (2.2%) and the uncertainties of the PDFs used in MC modeling (1.3%). The PDF uncertainty includes the error matrices of the CTEQ6.6 PDF sets and the differences between the CTEQ6.6 and the MSTW [21] PDF sets.

Cuts	ee Channel		$\mu\mu$ Channel		$e\mu$ Channel	
	$e\nu e\nu$	$\tau\nu\tau\nu$	$\mu\nu\mu\nu$	$\tau\nu\tau\nu$	$e\nu\mu\nu$	$\tau\nu\tau\nu$
Total Events	552.3	211.4	552.3	211.4	1104.5	423.1
2 leptons (SS+OS)	116.6	11.8	229.0	25.5	332.7	35.5
2 leptons (OS)	115.7	11.6	229.0	25.5	331.3	35.3
leading electron Pt > 25GeV	114.4	11.4	-	-	305.5	30.2
trigger matching	114.2	11.4	231.9	25.8	305.3	30.2
$M_{\ell\ell} > 15 \text{ GeV}$, $M_{e\mu} > 10 \text{ GeV}$	113.5	11.3	229.7	25.6	304.5	30.1
Z mass veto	88.2	8.4	176.6	19.0	-	-
$E_{\text{T, Rel}}^{\text{miss}}$ cut	38.6	2.9	69.7	5.2	193.2	16.1
Jet veto (No. of Jet=0)	27.8	1.7	49.4	3.1	139.6	10.9
W^+W^- Acceptance	5.0%	0.8%	8.9%	1.5%	12.6%	2.6%

Table I: W^+W^- MC event selection cut flow and overall acceptance. The MC W^+W^- signal expectations are normalized to 1.02 fb^{-1} integrated luminosity, using the NLO SM cross sections. ℓ refers to e , μ and τ in this table.

The systematic uncertainties on the W^+W^- signal acceptance are summarized in Table II, which gives the sources and associated uncertainties in W^+W^- signal acceptance for the ee , $\mu\mu$ and $e\mu$ channels.

5. Background estimation

The main backgrounds for the W^+W^- signal come from Drell-Yan events, top ($t\bar{t}$ and single top), W +jets, and diboson (WZ , ZZ , $W\gamma$ and $Z\gamma$) production, as described in this section.

Drell-Yan events ($Z/\gamma^* \rightarrow \ell^+\ell^-$), like W^+W^- events, produce two high p_{T} leptons. Much of this background is removed by the di-lepton invariant mass cuts and $E_{\text{T, Rel}}^{\text{miss}}$ cuts. Given the relatively large cross section of the Drell-Yan process, it contributes a non-negligible background to the W^+W^- signal due to energy/momentum mis-measurements of the two leptons or as a result of hadronic activity in the rest of the event. Extra pileup collisions are a significant contribution to this hadronic activity.

The Drell-Yan backgrounds are determined from MC events generated with ALPGEN and passed through the ATLAS detector simulation. The systematic uncertainties are determined using a data-driven method which compares the $E_{\text{T, Rel}}^{\text{miss}}$ distributions in data and MC within the Z peak region. The distributions are found to be consistent within statistical uncertainties. As a conservative estimate of the systematic, the observed difference is added in quadrature with the statistical uncertainty. This systematic uncertainty is applied to the background

Sources	$e^+e^- E_T^{\text{miss}}$	$\mu^+\mu^- E_T^{\text{miss}}$	$e^\pm\mu^\mp E_T^{\text{miss}}$
Luminosity	3.7%	3.7%	3.7%
Cross-section (theory)	5%	5%	5%
PDF	1.2%	1.4%	1.4%
Trigger	1.0%	1.0%	1.0%
Lepton p_T smearing	0.2%	0.1%	0.1%
Reco eff. scale factors	1.4%	0.0%	0.7%
E_T/p_T scale correction	0.9%	0.0%	0.4%
Particle ID eff. scale factors	3.3%	1.4%	1.6%
Isolation	4.0%	2.0%	3.0%
$E_{T, \text{Rel}}^{\text{miss}}$ in-time contribution	3.5%	3.9%	1.4%
$E_{T, \text{Rel}}^{\text{miss}}$ out-of-time contribution	0.5%	0.5%	0.3%
Jet-veto	4.8%	4.8%	4.8%
Total experimental uncertainty	8.1%	6.7%	6.2%
Overall uncertainty for WW signal estimation	10.3%	9.2%	8.9%

 Table II: Uncertainty sources and associated relative uncertainties for WW signal for the ee , $e\mu$ and $\mu\mu$ channels.

predictions from MC. With the assumptions that the mechanism that causes a discrepancy between data and MC is independent of the invariant mass of the two leptons, and that any discrepancy between data and MC is caused by a mis-modeling of the Drell-Yan sample, a systematic uncertainty of 10.4% for the Drell-Yan background estimation from the MC simulation is determined. The estimated Drell-Yan backgrounds together with statistical and systematic uncertainties are shown in Table III.

After removing the largest background from $Z/\gamma^* \rightarrow \ell^+\ell^-$ events in di-lepton samples, the dominant background is from $t\bar{t}$ and Wt , followed by the leptonic decays of two real W bosons. This background can be effectively suppressed by requiring that there are no jets with $p_T > 30$ GeV and $|\eta| < 4.5$. However, some top events containing only jets with p_T less than 30 GeV can still mimic the SM W^+W^- events.

The top backgrounds in the final W^+W^- selection are estimated using a data driven method which is cross-checked with the Monte Carlo simulation. In this method, the top background in the zero jet bin is estimated using the number of observed events in the N -jet bins (where $N \geq 2$) in data and the ratio of zero-jet events over the number of N -jet events in MC, $N_{\text{top}}^{\text{zero-jet}}(\text{estimate}) = N_{\text{data}}^{\geq 2\text{-jets}} \times (N_{\text{MC top}}^{\text{zero-jet}}/N_{\text{MC top}}^{\geq 2\text{-jets}})$. The uncertainties on luminosity and on the top cross sections cancel out in the MC ratio. A second method uses a top control sample selected using b -tagging to estimate the top contribution. Both data-driven methods give top background yields consistent with MC and with each other. The final top background estimated is $58.6 \pm 2.1(\text{stat}) \pm 22.3(\text{syst})$ events, the systematic uncertainty is dominated by the jet-energy scale uncertainty (37%).

W bosons produced in association with a hadronic jet give rise to W^+W^- backgrounds when the jet is misidentified as a lepton. The rate at which hadronic jets are misidentified as leptons may not be accurately described in the MC. The $W+$ jets background is therefore determined from data. The $W+$ jet background is estimated by defining a control region, similar to the W^+W^- signal selection, that is enriched in $W+$ jet events. The $W+$ jet control region is defined using an alternative lepton definition that is rich in hadronic jets. Jet-rich electrons are defined as isolated electromagnetic clusters matched to a track in the inner detector that fail the **medium** [14] electron identification requirements. Jet-rich muons are defined as ‘‘combined’’ muons that pass a looser isolation requirement and fail the muon selection. Events containing one fully identified lepton and a jet passing this jet-rich lepton definition are selected. These events are then required to pass the full W^+W^- event selection, where the jet is treated as if it were a fully identified lepton. The $W+$ jets background is estimated by scaling the control sample ($N_{W+\text{jet}}$) by a measured fake factor. The fake factor (f) is defined as the ratio of the rate at which jets satisfy the full lepton identification to the rate at which they satisfy the jet-enriched lepton selection. The fake factor is measured in a di-jet data sample, parametrized as a function of lepton p_T , and is found to be 0.02 (0.25) for electrons (muons) in the 30-40 GeV region. The $W+$ jets background is determined as $N_{W+\text{jet}} \times f$. Samples with same sign di-leptons are also enhanced in $W+$ jets events and are used as a control sample, with looser lepton identification, to cross check the method described above. The $W+$ jets prediction based on the fake factor method agrees well with the observed same sign di-lepton data. The $W+$ jets background estimation in the W^+W^- signal region is given in Table III for the three di-lepton channels. The statistical uncertainty is due to the limited statistics in the $W+$ jet control

regions. The systematic uncertainty is due to the uncertainty on the determination of f . The uncertainty on f is about 30% for both electrons and muons, and is determined by the measured variations of f in different run periods and in data samples containing jets of different energies. The assigned systematic uncertainty covers variation of the quark/gluon composition of the jets in the jet data sample compared to jets in the W + jets sample, and the effects of changing instantaneous luminosity on f . The total W + jets contribution to the final selected WW candidate events is estimated to be $50.5 \pm 4.8(\text{stat}) \pm 14.7(\text{syst})$.

Other backgrounds to W^+W^- originate from the diboson processes WZ , ZZ and $W+\gamma$. The leptonic decays of WZ and ZZ events can mimic the W^+W^- signal when one or more of the charged leptons is not reconstructed and instead contributes to E_T^{miss} . The $ZZ \rightarrow \ell\ell\nu\nu$ process is suppressed by the Z veto cut. The $W\gamma$ process is a background only for the ee and $e\mu$ channels, since the probability for a photon to be misidentified as a muon is negligible. These diboson background contributions are estimated using MC simulations (MC@NLO for WZ , PYTHIA for ZZ and PYTHIA/MADGRAPH for $W+\gamma$). The total diboson background contribution is estimated to be $6.8 \pm 0.4(\text{stat}) \pm 0.8(\text{syst})$ events for 1.02 fb^{-1} of integrated luminosity. The quoted systematic uncertainty includes uncertainties in the luminosity (3.7%), the SM diboson cross-sections (5%), the jet veto efficiency (9.6%), the di-lepton trigger and identification efficiencies (4.5%) and E_T^{miss} uncertainty (2.2%). The hadronic dijets background contribution is negligible in the W^+W^- signal region as determined by PYTHIA MC and cross-checked by data.

6. WW Production and Fiducial Cross Sections

The observed and expected number of events after applying all W^+W^- selection cuts are shown in Table III. Both statistical and systematic uncertainties are given for all three di-lepton channels in the table. The kinematic distributions of the final W^+W^- candidates together with the predicted W^+W^-

Final State	$e^+e^- E_T^{\text{miss}}$	$\mu^+\mu^- E_T^{\text{miss}}$	$e^\pm\mu^\mp E_T^{\text{miss}}$	Combined
Observed Events	74	97	243	414
Background estimations				
Top(data-driven)	$9.5 \pm 0.3 \pm 3.6$	$12.3 \pm 0.4 \pm 4.7$	$36.8 \pm 1.3 \pm 14.0$	$58.6 \pm 2.1 \pm 22.3$
W+jets (data-driven)	$5.3 \pm 0.4 \pm 1.7$	$12.4 \pm 2.9 \pm 5.2$	$32.9 \pm 3.8 \pm 9.2$	$50.5 \pm 4.8 \pm 14.7$
Drell-Yan (MC/data-driven)	$18.7 \pm 1.9 \pm 1.9$	$19.2 \pm 1.7 \pm 2.1$	$16.0 \pm 2.8 \pm 1.7$	$54.0 \pm 3.7 \pm 4.5$
Other dibosons (MC)	$0.9 \pm 0.1 \pm 0.1$	$2.4 \pm 0.2 \pm 0.3$	$3.4 \pm 0.3 \pm 0.4$	$6.8 \pm 0.4 \pm 0.8$
Total Background	$34.4 \pm 2.0 \pm 4.4$	$46.3 \pm 3.4 \pm 7.3$	$89.1 \pm 4.9 \pm 16.8$	$169.8 \pm 6.4 \pm 27.1$
Expected WW Signal	$29.5 \pm 0.3 \pm 3.0$	$52.5 \pm 0.4 \pm 4.9$	$150.5 \pm 0.7 \pm 13.4$	$232.4 \pm 0.9 \pm 21.5$
Significance (S/\sqrt{B})	5.0	7.7	15.9	17.8

Table III: Summary of observed events and expected signal and background contributions in the three di-lepton and combined channels. The first error is statistical, the second systematic. The central value and statistical uncertainty for the Drell-Yan process estimation is MC based while the systematic uncertainties are derived from a data-driven method.

signal and estimated background are shown in Figures 2. The distributions of transverse mass $M_T = \sqrt{(E_T^{\ell 1} + E_T^{\ell 2} + E_T^{\text{miss}})^2 - (\vec{p}_T^{\ell 1} + \vec{p}_T^{\ell 2} + \vec{E}_T^{\text{miss}})^2}$ and transverse momentum $p_T(\ell\ell E_T^{\text{miss}})$ of the di-lepton plus E_T^{miss} system, where E_T^ℓ and \vec{p}_T^ℓ denote transverse energies and momenta for leptons, and E_T^{miss} and \vec{E}_T^{miss} denote missing transverse energy and momentum in the event. The MC distributions in these plots are normalized to the integrated luminosity of 1.02 fb^{-1} and the SM cross sections with event selection acceptance. The data agree reasonably well with the estimated signal and background.

The total and fiducial W^+W^- production cross sections are determined from the three dilepton channels ($WW \rightarrow e\nu e\nu$, $\mu\nu\mu\nu$ and $e\nu\mu\nu$) by maximizing the log-likelihood functions shown in Equation 2 and 3, respectively:

$$L(\sigma_{WW}^{\text{tot}}) = \ln \prod_{i=1}^3 \frac{e^{-(N_s^i + N_b^i)} \times (N_s^i + N_b^i)^{N_{obs}^i}}{N_{obs}^i!}, \quad N_s^i = \sigma_{WW}^{\text{tot}} \times Br^i \times \mathcal{L} \times \epsilon_{WW}^i \quad (2)$$

$$L(\sigma_{WW}^{\text{fid}}) = \ln \frac{e^{-(N_s^i + N_b^i)} \times (N_s^i + N_b^i)^{N_{obs}^i}}{N_{obs}^i!}, \quad N_s^i = \sigma_{WW \rightarrow \ell\nu\ell\nu}^i \times \mathcal{L} \times C_{WW}^i \quad (3)$$

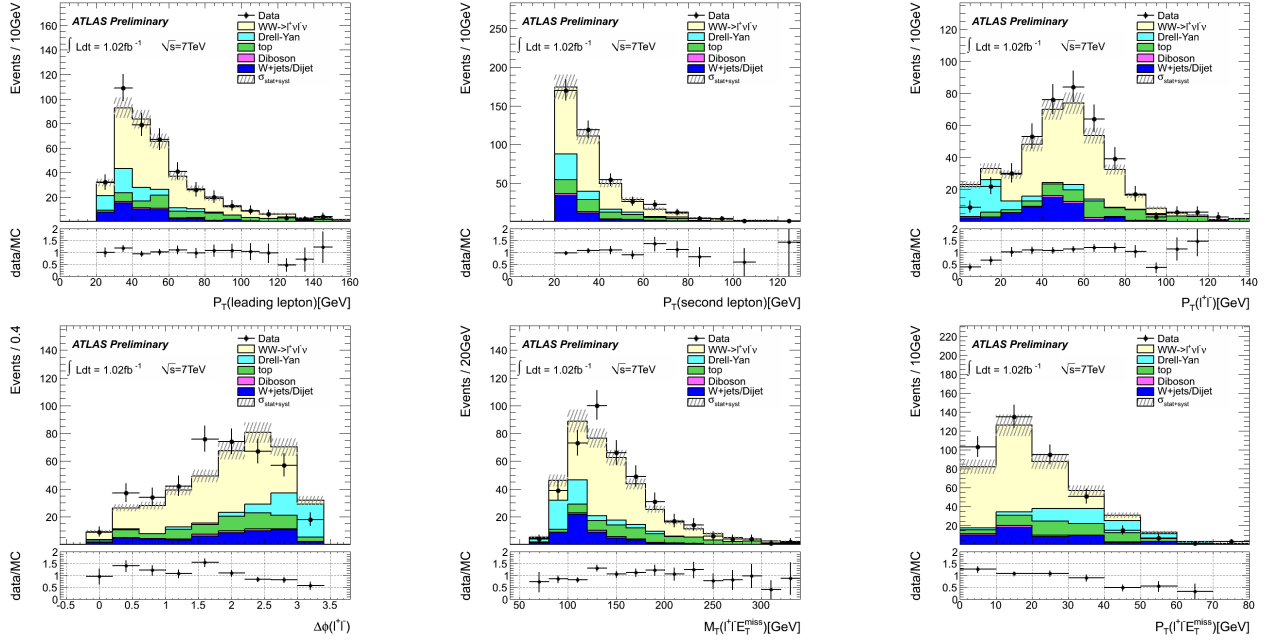


Figure 2: Distributions of leading (top left), sub-leading (top middle) lepton p_T and di-lepton system p_T (top right) for W^+W^- candidates. Distributions of $\Delta\phi(\ell^+\ell^-)$ (bottom left), WW transverse mass (bottom middle) and p_T of WW (bottom right). The points are data and stacked histograms are from MC predictions except the W +jets background (from data-driven methods). The estimated uncertainties are shown as the hatched bands (stat \oplus syst).

where $i = 1, 2, 3$ runs over the three dilepton channels. N_s^i , N_b^i and N_{obs}^i represent the SM expected signal, estimated background events and observed data events for the i -th dilepton channel while Br^i is the branching ratio (including the contribution via τ decays) and \mathcal{L} is the total integrated luminosity. The overall correction factor required to evaluate the fiducial cross section is defined as C_{WW} , and takes into account the detector resolution, efficiency and background corrections relating the reconstructed event selection to the true particle-level phase space region defining the cross section. The overall detector acceptance described in the total cross section measurement section relates the fiducial phase space acceptance A_{WW} and the correction factor C_{WW} : $\epsilon_{WW} = A_{WW} \times C_{WW}$. Table I gives the overall efficiencies for prompt ee , $\mu\mu$ and $e\mu$ decays from W^+W^- . It also gives the detection efficiencies involving the electron or muon decay from τ s.

The mean values of the total W^+W^- cross sections obtained from the log-likelihood maximization are listed in Table IV, and they are consistent with the SM NLO prediction for W^+W^- production of 46 ± 3 pb. The statistical uncertainty is determined from the likelihood fit, and the systematic uncertainty of our measurement is 13.4%, which includes the signal acceptance uncertainty ($\Delta\epsilon_{WW}/\epsilon_{WW}$) of 6.8% and the uncertainty on the background estimation ($\Delta N_{bkg}/(N_{obs} - N_{bkg})$) of 11.5%. The systematic error is calculated using error propagation: $(\Delta\sigma/\sigma)_{syst} = \sqrt{((\Delta\epsilon_{WW}/\epsilon_{WW})^2 + (\Delta N_{bkg}/(N_{obs} - N_{bkg}))^2)}$. The systematic uncertainties on the cross section measurements from each dilepton channel are listed in Table IV. The luminosity contributes 3.7% systematic uncertainty to the cross-section measurements and it is listed separately in the table. By combining all three dilepton channels, the statistical error (8.3%) is smaller than the systematic uncertainty (13.4%) in this measurement.

Channels	Total cross-section (pb)	$\Delta\sigma_{stat}$ (pb)	$\Delta\sigma_{syst}$ (pb)	$\Delta\sigma_{lumi}$ (pb)
$e\nu e\nu$	62.1	± 13.5	± 9.1	± 2.3
$\mu\nu\mu\nu$	44.7	± 8.7	± 7.7	± 1.7
$e\nu\mu\nu$	47.3	± 4.8	± 6.2	± 1.8
Combined	48.2	± 4.0	± 6.4	± 1.8

Table IV: The measured total W^+W^- production cross sections in three dilepton channels.

In order to minimize the extrapolation from the measured to the theoretical cross section, the W^+W^- fiducial

phase space is defined using WW selection cuts on MC truth information. A_{WW} denotes the acceptance for the W^+W^- decays under consideration (including $\tau \rightarrow e/\mu + \nu\nu$ decays), defined as the fraction of decays satisfying the geometrical and kinematical constraints at the generator level (fiducial acceptance). It is defined here after the decay leptons emit photons via QED final state radiation; photons within a $\Delta R < 0.1$ cone are added back to the decay leptons (“dressed” leptons). C_{WW} denotes the ratios between the total number of generated events which pass the final selection requirements after reconstruction and the total number of generated events within the fiducial acceptance. This correction factor includes the efficiencies for triggering, reconstructing, and identifying the W^+W^- decays falling within the acceptance. The systematic uncertainty of A_{WW} is about 6.9%. It includes the parton distribution function uncertainty (1.2% for ee , 1.4% for $\mu\mu$ and $e\mu$), the renormalization and factorization scales uncertainty (5.3% for ee , 4.4% for $e\mu$ and 1.5% for $\mu\mu$) and the uncertainty due to the parton shower/fragmentation modeling difference between MC@NLO and MCFM NLO MC generators (4.8%). The MC scale uncertainty was evaluated using MC samples where the normalization and the factorization scales were changed to one half and to twice their nominal value.

The overall W^+W^- event selection efficiency can be presented as $A_{WW} \times C_{WW}$. Using the overall efficiencies for different channels shown in Table I, we can determine the C_{WW} once the A_{WW} are determined. The systematic uncertainties from various sources for C_{WW} are listed in Table II. The systematic uncertainty associated with the jet-veto cut, 4.8%, is replaced by a 4.5% JES uncertainty term. The systematic uncertainty on C_{WW} related to changes in the normalization and factorization scales is 1.9% in the ee channel, 2.9% in the $e\mu$ channel, and 5.1% in the $\mu\mu$ channel. A total cross section measurement requires the evaluation of the systematic on $A_{WW} \times C_{WW}$, for which the systematics on A_{WW} and C_{WW} partially overlap. Table V gives the fiducial phase space acceptance A_{WW} and the correction factor C_{WW} for all three dilepton channels.

Channels	$A_{WW} \times C_{WW}$	A_{WW}	C_{WW}
$e\nu e\nu$	$0.039 \pm 0.001 \pm 0.004$	$0.090 \pm 0.001 \pm 0.007$	$0.432 \pm 0.006 \pm 0.035$
$\mu\nu\mu\nu$	$0.069 \pm 0.001 \pm 0.006$	$0.086 \pm 0.001 \pm 0.005$	$0.802 \pm 0.006 \pm 0.066$
$e\nu\mu\nu$	$0.100 \pm 0.001 \pm 0.008$	$0.167 \pm 0.001 \pm 0.011$	$0.596 \pm 0.005 \pm 0.040$

Table V: The WW overall acceptance $A_{WW} \times C_{WW}$, fiducial phase space acceptance A_{WW} and correction factor C_{WW} . The first errors mean statistical errors and the second errors represent systematic errors.

Channels	expected σ^{fid} (fb)	measured σ^{fid} (fb)	$\Delta\sigma_{stat}$ (fb)	$\Delta\sigma_{syst}$ (fb)	$\Delta\sigma_{lumi}$ (fb)
$e\nu e\nu$	66.8	90.1	± 18.9	± 11.3	± 3.3
$\mu\nu\mu\nu$	63.8	62.0	± 12.1	± 10.7	± 2.3
$e\nu\mu\nu$	245.1	252.0	± 24.6	± 29.4	± 9.3

Table VI: The predicted and measured fiducial W^+W^- production cross sections.

7. Summary

The W^+W^- production cross section in pp collisions at $\sqrt{s} = 7$ TeV is measured using three W^+W^- leptonic decay channels and 1.02 fb^{-1} of data collected by the ATLAS detector during 2011. A total of 414 candidates are selected with an estimated background of 170 ± 28 events. The measured cross section is $48.2 \pm 4.0(\text{stat}) \pm 6.4(\text{syst}) \pm 1.8(\text{lumi}) \text{ pb}$, consistent with the SM NLO prediction of $46 \pm 3 \text{ pb}$.

Acknowledgments

The author would like to thank CERN for the very successful operation of the LHC and the ATLAS Collaboration for excellent work on the Monte Carlo simulation and the software package for physics analysis. The author is supported by the Department of Energy (DE-FG02-95ER40899) of the United States.

References

- 1 ATLAS Collaboration, Phys. Rev. Lett. 107, 041802 (2011).
- 2 ATLAS Collaboration, JINST 3 (2008) S08003.
- 3 ATLAS Collaboration, ATLAS-CONF-2011-011.
- 4 S. Frixione and B. R. Webber, JHEP 06 (2002) 029, hep-ph/0204244.
- 5 P. M. Nadolsky et al., Phys. Rev. D78 (2008) 013004, arXiv:0802.0007 [hep-ph].
- 6 G. Corcella et al., JHEP 0101 (2001) 010, arXiv:hep-ph/0011363.
- 7 J. M. Butterworth et al., Z. Phys. C72 (1996) 637–646.
- 8 T. Binoth, M. Ciccolini, N. Kauer, and M. Kramer, JHEP 12 (2006) 046, arXiv:hep-ph/0611170.
- 9 T. Sjostrand et al., Comput. Phys. Commun. 135 (2001) 238–259, arXiv:hep-ph/0010017.
- 10 B. P. Kersevan and E. Richter-Was, arXiv:hep-ph/0405247.
- 11 J. Alwall et al., JHEP 09 (2007) 028, arXiv:0706.2334 [hep-ph].
- 12 ATLAS Collaboration, Eur.Phys.J. C70 (2010) 823–874, arXiv:1005.4568 [physics.ins-det].
- 13 S. Agostinelli et al., *GEANT4: A Simulation toolkit*, Nucl.Instrum.Meth. A506 (2003) 250–303.
- 14 ATLAS Collaboration, JHEP 12 (2010) 060, arXiv:1010.2130 [hep-ex].
- 15 M. Cacciari, G. P. Salam, and G. Soyez, JHEP 04 (2008) 063, arXiv:0802.1189 [hep-ph].
- 16 M. Cacciari and G. P. Salam, Phys. Lett. B641 (2006) 57–61, arXiv:hep-ph/0512210.
- 17 M. Cacciari, G. P. Salam, G. Soyez, <http://fastjet.fr/>.
- 18 ATLAS Collaboration, ATLAS-CONF-2011-032.
- 19 J. M. Campbell et al., Phys. Rev. D80 (2009) 054023, arXiv:0906.2500 [hep-ph].
- 20 J. M. Campbell and R. K. Ellis, Phys. Rev. D62 (2000) 114012, arXiv:hep-ph/0006304.
- 21 A. D. Martin et al., Eur. Phys. J. C63 (2009) 189–285, arXiv:0901.0002 [hep-ph].